Desalination and Water Treatment
www.deswater.com
doi: 10.1080/19443994.2014.932709

56 (2015) 107–120
September

Taylor & Francis
Taylor & Francis Group

Amine functionalized magnetic carbon nanotube: synthesis and binary system dye removal

Niyaz Mohammad Mahmoodi*, Farzaneh Bagherpour, Elham Nariyan

Department of Environmental Research, Institute for Color Science and Technology, Tehran, Iran, Tel. +98 021 22969771; Fax: +98 021 22947537; emails: mahmoodi@icrc.ac.ir, nm_mahmoodi@aut.ac.ir, nm_mahmoodi@yahoo.com (N.M. Mahmoodi); farzan.1362@yahoo.com (F. Bagherpour); elham_136415@yahoo.com (E. Nariyan)

Received 16 November 2013; Accepted 2 June 2014

ABSTRACT

In this paper, the amine functionalized magnetic carbon nanotube (AFMCNT) was synthesized and used to remove anionic dyes from single and binary systems. The characteristics of AFMCNT were investigated using Fourier transform infrared and scanning electron microscope. Acid Blue 92 (AB92), Acid Red 14 (AR14), and Direct Red 31 (DR31) were used as anionic dyes. The effect of operational parameters (AFMCNT dosage and pH) on dye removal was investigated. The adsorption isotherm and kinetics were studied. The isotherm data in single and binary systems followed Langmuir isotherm. The maximum adsorption capacity (Q_0) of AB92, AR14, and DR31 was 333, 370, and 323 mg/g, respectively. Dye adsorption kinetics in single and binary systems followed pseudo-second-order kinetics model. The results showed that AFMCNT was an effective adsorbent to remove cationic dyes from binary systems.

Keywords: Amine functionalization; Magnetic carbon nanotube; Synthesis; Binary system dye removal

1. Introduction

Textile industry use dyes to color its products and consumes substantial volume of water. It is estimated to be more than 100,000 commercially available dyes and some of them are known to be toxic due to the production of harmful byproducts. Thus, there is need to have a method, which may work suitably and should be cost effective for the dye removal. Adsorption process is one of the different wastewater treatment processes [1–9].

Carbon nanotube (CNT) as an adsorbent removes different pollutants such as trihalomethanes [10], microcystins [11], fluoride [12], lead [13], nickel [14], and arsenate [15] that are present in natural water resources [16,17]. An emerging field in adsorption process is the application of magnetic adsorbents to remove pollutants [18,19]. The magnetic adsorbents could be separated based on their structures since the ease of direction of magnetisation would vary depending on the ordering of atoms in the magnetic structure [18,20]. Some magnetic adsorbents have low adsorption capacity due to the repulsion forces between the adsorbent and adsorbate. Thus, the surface of adsorbent should be modified. The properties of surface-modified adsorbents have opened a new field in engineering separations applications due to relatively high adsorption capacity.

*Corresponding author.

A literature review showed that the amine functionalized magnetic multiwalled carbon nanotube (AFMCNT) was not investigated to remove anionic dyes from binary system. AFMCNT was synthesized and used to remove anionic dyes from single (sin.) and binary (bin.) systems (Fig. 1). The characteristics of AFMCNT were investigated using Fourier transform infrared (FTIR) and scanning electron microscope (SEM). Acid Blue 92 (AB92), Acid Red 14 (AR14), and Direct Red 31 (DR31) were used as anionic dyes. The effective parameters (AFMCNT dosage and pH), isotherm and kinetics studies were investigated to evaluate the dye removal ability of AFMCNT from single and binary systems. The Langmuir, Freundlich, and Temkin isotherms were used to fit the equilibrium data. The pseudo-first-order, pseudo-second-order, and intraparticle diffusion kinetics models were attempted.

2. Experimental

2.1. Materials

The multiwalled carbon nanotube (appearance: black powder, number of walls: 3–15, specific surface area (BET, N_2): 240 m^2/g, and outer diameter/inner diameter/length: 5–20/2–6/1–10 μm) was purchased from PlasmaChem GmbH (Germany). Anionic dyes were Acid Blue 92 (AB92), Acid Red 14 (AR14), and Direct Red 31 (DR31). The dyes were obtained from Ciba and used without further purification. The chemical structure of dyes is shown in Fig. 2. All other chemicals were purchased from Merck (Germany).

2.2. Synthesize of AFMCNT

2.2.1. Magnetic carbon nanotube

Manganese nitrate (5 g) and iron nitrate (13.4 g) were dissolved in distilled water (50 mL) and added to aqueous mixed solution of multiwalled carbon nanotube (1 g), NaOH (4.2 g) in distilled water (70 mL), and ethylene diamine (3 mL). This solution was heated at 90˚C for 1 h to achieve complete chelation. The powder was calcined on alumina crucible at 500˚C for 1 h, with a heating rate of 10˚C/min.

2.2.2. AFMCNT

Magnetic carbon nanotube (MCNT) (1 g) and (3-aminopropyl) trimethoxy silane (2 g) were poured

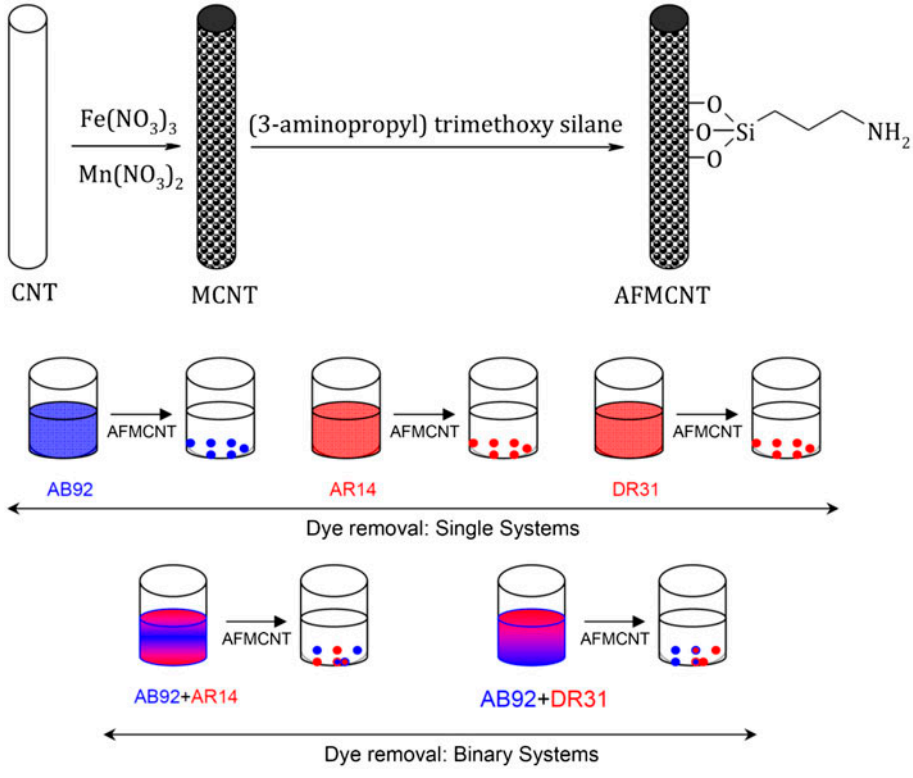

Fig. 1. Synthesis of AFMCNT and its dye removal ability from single and binary systems.

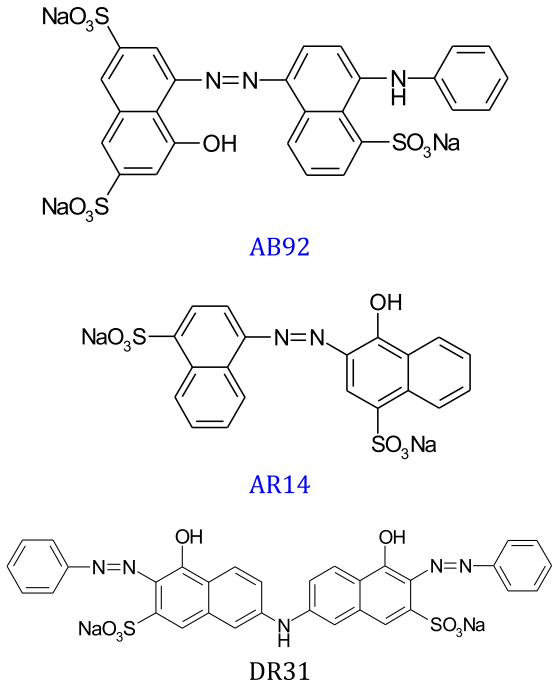

Fig. 2. The chemical structure of anionic dyes.

into a mixture of water, acetone, and nonionic surfactant and mixed for 4 h at 25°C. The precipitate was filtered, washed with deionized water, and dried.

2.3. Characterization

The functional group of the materials was studied using FTIR spectroscopy (Perkin-Elmer Spectrophotometer Spectrum One) in the range of 4,000–450 cm^{-1}. The morphological structure of the materials was examined by SEM using a LEO 1455VP scanning microscope.

2.4. Dye removal

The dye adsorption measurements were done by the mixing of AFMCNT in single and binary systems of dyes in jars containing 250 mL of a dye solution (100 mg/L). Experiments were carried out at different dye concentrations using AFMCNT for single and binary systems at 25°C for 60 min to attain equilibrium conditions. After experiments, the AFMCNT was separated by magnetic force from solution samples and then the dye concentration was determined. The changes of absorbance were determined at certain time intervals (2.5, 5, 7.5, 10, 15, 20, 25, 30, 40, 50, and 60 min) during the adsorption process using UV–vis Perkin-Elmer Lambda 25 spectrophotometer. The maximum wavelength (λ_{max}) of AB92, AR14, and DR31 to determine residual dye concentration in solution was 571, 517, and 530 nm, respectively.

Dye concentrations in a binary system of components A and B at wavelengths of λ_1 and λ_2, respectively, to give optical densities of d_1, and d_2 were measured as follows [21]:

$$d_1 = k_{A1}C_A + k_{B1}C_B \quad (1)$$

$$d_2 = k_{A2}C_A + k_{B2}C_B \quad (2)$$

$$C_A = \left(\frac{k_{B2}d_1 - k_{B1}d_2}{k_{A1}k_{B2} - k_{A2}k_{B1}}\right) \quad (3)$$

$$C_B = \left(\frac{k_{A1}d_2 - k_{A2}d_1}{k_{A1}k_{B2} - k_{A2}k_{B1}}\right) \quad (4)$$

where k_{A1}, k_{B1}, k_{A2}, and k_{B2} are the calibration constants for components A and B at the two wavelengths λ_1 and λ_2, respectively.

The effect of adsorbent dosage (0.025–0.1 g) on dye removal from single (sin.) and binary (bin.) systems was investigated by contacting 250 mL of dye solution with initial dye concentration of 100 mg/L at room temperature (25°C) for 60 min.

The effect of pH (2, 4, 6, and 10) on dye removal from single (sin.) and binary (bin.) systems was investigated by contacting 250 mL of dye solution with initial dye concentration of 100 mg/L, AFMCNT at room temperature (25°C) for 60 min.

3. Results and discussion

3.1. Characterization

The FTIR spectra of CNT and MCNT in the wavelength ranges from 4,000 to 400 cm^{-1} is shown in Fig. 3. The FTIR spectrum of CNT (Fig. 3(a)) shows that the peak position is at 3,422 cm^{-1} due to OH stretching. In FTIR spectrum of MCNT (Fig. 3(b)), a broad absorption band around 3,400 cm^{-1} and less intensive band at 1,620 cm^{-1} are attributed to the stretching vibration of the hydrogen-bonded O–H groups [22–24]. The absorption band around 500 and 600 cm^{-1} due to the metal-oxygen bonds is observed [25–28]. In FTIR spectrum of AFMCNT (Fig. 3(c)), an absorption band around 1,000 cm^{-1} is attributed to the stretching vibration of the Si–O groups.

SEM is used to characterize the surface morphology and fundamental physical properties of material surface. It is applicable for determining the particle

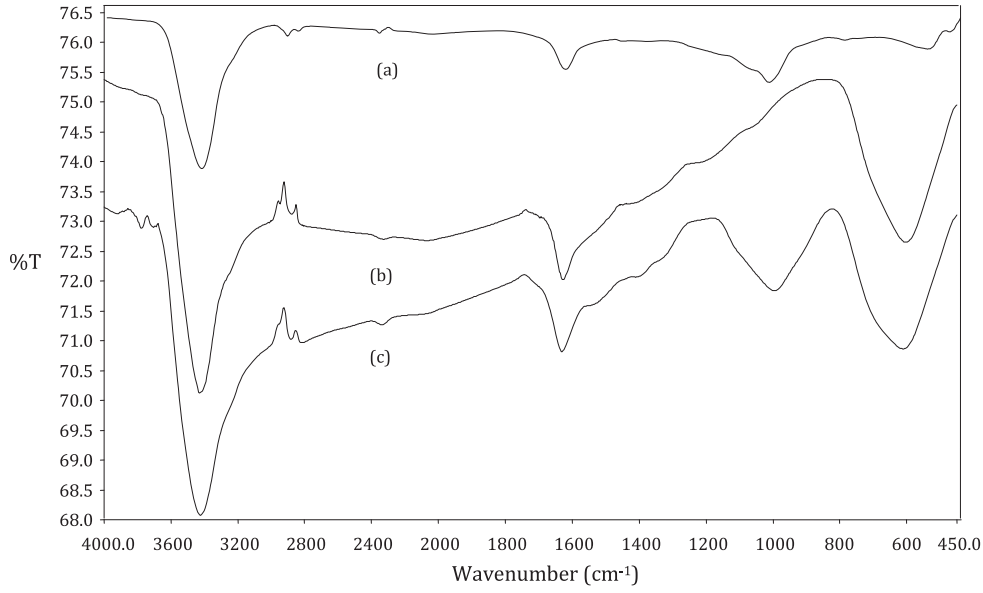

Fig. 3. FTIR spectrum (a) CNT, (b) M-CNT, and (c) AFMCNT.

shape, particle size distribution, etc. The SEM micrographs of the CNT, MCNT, and AFMCNT (Fig. 4) shows a relatively homogeneous amine functionalization of MCNT.

3.2. Adsorption isotherm

In order to design an effective adsorption system to remove dyes from solutions, it is important to establish the most appropriate correlation for the equilibrium curve. Many models have been used in literature to describe the experimental data of adsorption isotherms. The Langmuir model is the most frequently employed model and given by [29,30]:

$$\frac{C_e}{q_e} = \frac{1}{K_L Q_0} + \frac{C_e}{Q_0} \tag{5}$$

where C_e, q_e, Q_0, and K_L are the concentrations of adsorbate at equilibrium (mg/L), the amount of dye adsorbed at equilibrium (mg/g), maximum adsorption capacity(mg/g), and Langmuir constant (mg/L), respectively.

To study the applicability of the Langmuir isotherm for the dye adsorption onto AFMCNT in single system, linear plot of C_e/q_e against C_e is plotted. The values of Q_0, K_L, and R^2 (correlation coefficient values of all isotherms models) are shown in Table 1.

The Freundlich isotherm is derived by assuming a heterogeneous surface with a non-uniform distribution of heat of adsorption over the surface. Freundlich isotherm can be expressed by [31]:

$$\log q_e = \log K_F + (1/n)\log C_e \tag{6}$$

where K_F is adsorption capacity at unit concentration and $1/n$ is adsorption intensity. $1/n$ values indicate the type of isotherm to be irreversible ($1/n = 0$), favorable ($0 < 1/n < 1$), and unfavorable ($1/n > 1$) [32]. The $1/n$ values for the Freundlich adsorption isotherm are shown in Table 1.

To study the applicability of the Freundlich isotherm for the dye adsorption onto AFMCNT, linear plots of log q_e vs. log C_e is plotted. The values of K_F, $1/n$, and R^2 (correlation coefficient) are shown in Table 1.

Temkin isotherm contains a factor that explicitly takes into account the adsorbing species adsorbent interactions. This isotherm assumes the heat of adsorption of all the molecules in the layer which decreases linearly with coverage due to adsorbent–adsorbate interactions, and the adsorption is characterized by a uniform distribution of binding energies, up to some maximum binding energy [33,34]. The Temkin isotherm is given as [33]:

$$q_e = B_1 \ln K_T + B_1 \ln C_e \tag{7}$$

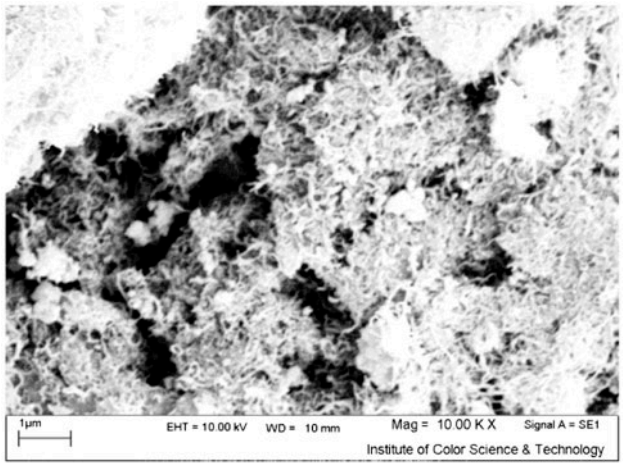

(a)

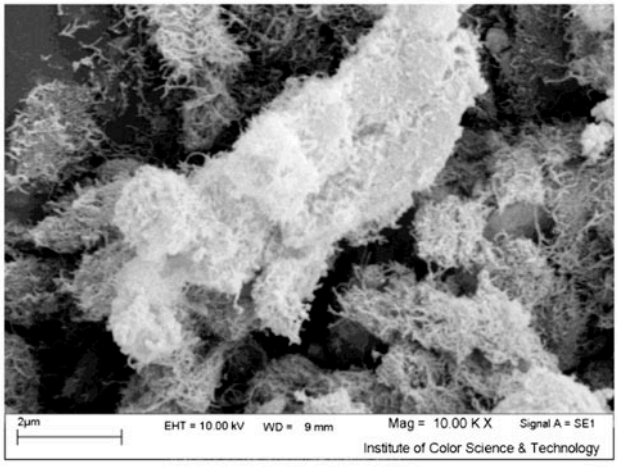

(b)

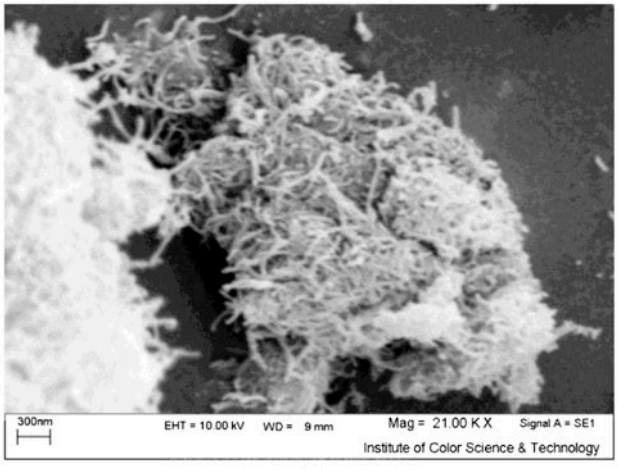

(c)

Fig. 4. SEM image (a) CNT, (b) MCNT, and (c) AFMCNT.

where

$$B_1 = \frac{RT}{b} \tag{8}$$

where R and T are the gas constant (8.314 J/mol K) and the absolute temperature (K), respectively.

A plot of q_e vs. ln C_e enables the determination of the isotherm constants B_1 and K_T from the slope and the intercept, respectively. K_T is the equilibrium binding constant (L/mol) corresponding to the maximum binding energy and constant B_1 is related to the heat of adsorption (Table 1).

To study the applicability of the Temkin isotherm for the dye adsorption onto AFMCNT, linear plot q_e vs. ln C_e is plotted. The values of K_T, B_1, and R^2 (correlation coefficient) are shown in Table 1.

The correlation coefficient values (R^2) show that the dye removal isotherm using AFMCNT does not follow the Freundlich and Temkin isotherms (Table 1). The linear fit between the C_e/q_e vs. C_e and calculated correlation coefficients (R^2) for Langmuir isotherm model show that the dye removal isotherm can be approximated as Langmuir model (Table 1). This means that the adsorption of dyes takes place at specific homogeneous sites and a one layer adsorption onto AFMCNT surface.

The maximum adsorption capacity of different CNTs for anionic dyes is shown in Table 2 [35–38]. The results show that AFMCNT has high dye adsorption capability. Thus AFMCNT can be used as a high capacity adsorbent to remove anionic dyes.

3.3. Adsorption kinetics

The mechanism of solute adsorption onto an adsorbent was studied by kinetics models. Several models were used. In order to design a fast and effective model, investigations were made on adsorption rate. For the examination of the controlling mechanisms of adsorption process, such as chemical reaction, diffusion control and mass transfer, several kinetics models are used to test the experimental data [6,39].

Pseudo-first-order equation is generally represented as follows [40]:

$$\log(q_e - q_t) = \log(q_e) - (k_1/2.303)t \tag{9}$$

where q_t and k_1 are the amount of dye adsorbed at time t (mg/g) and the equilibrium rate constant of pseudo-first-order kinetics (1/min), respectively.

The straight-line plots of $\log(q_e - q_t)$ vs. t for the dye adsorption of single and binary systems onto AFMCNT have also been tested to obtain the rate parameters (Fig. 5). The k_1, the experimental q_e

Table 1
Linearized isotherm coefficients of dye removal using AFMCNT at different adsorbent dosages from single and binary systems

System			Langmuir			Freundlich			Temkin		
			Q_0	K_L	R^2	K_F	$1/n$	R^2	K_T	B_1	R^2
Single system		AB92									
		333	0.170	0.992	167	0.142	0.890	44	38	0.875
		AR14									
		370	0.313	0.998	205	0.13	0.962	164	38	0.955
		DR31									
		323	0.164	0.992	164	0.1405	0.890	45	37	0.875
Binary system	AB92 + AR14	AB92									
		357	0.071	0.995	88	0.289	0.942	1	71	0.951
		AR14									
		323	0.021	0.944	26	0.473	0.906	1	83	0.916
	AB92 + DR31	AB92									
		238	0.285	0.999	156	0.903	0.962	1843	19	0.967
		DR31									
		278	0.324	0.999	173	0.106	0.925	2	260	0.936

Table 2
Adsorption capacity of different carbon nanotubes to remove anionic dyes

Adsorbent	Adsorbate	Q_0 (mg/g)	References
CNT	Acid Red 183	45.2	[35]
CNT	Acid Red 18	166.7	[36]
CNT	Reactive Blue 4	69.0	[37]
	Acid Red 183	45.0	
M-MWCNT–Fe3C nanocomposite	Direct Red 23	85.5	[38]
AFMCNT	Acid Blue 92	333	Present study
	Acid Red 14	370	
	Direct Red 31	323	

($(q_e)_{Exp}$), and correlation coefficients under different dye concentrations values were calculated from these plots and are given in Table 3.

Data were applied to the pseudo-second-order kinetics rate equation which is expressed as [41]:

$$\frac{t}{q_t} = \frac{1}{kq_e^2} + \left(\frac{t}{q_e}\right)^t \quad (10)$$

where k_2 is the equilibrium rate constant of pseudo-second order (g/mg/min).

To understand the applicability of the model, linear plots of t/q_t vs. t for the adsorption of dyes in single and binary system onto AFMCNT are plotted (Fig. 6). The k_2, the experimental q_e ($(q_e)_{Exp}$), and correlation coefficients were calculated from these plots and are given in Table 3.

The possibility of intraparticle diffusion resistance affecting adsorption was explored by using the intraparticle diffusion model as [42,43]:

$$q_t = k_p t^{1/2} + I \quad (11)$$

where k_p is the intraparticle diffusion rate constant.

To understand the applicability of the intraparticle diffusion model, linear plots of q_t vs. $t^{1/2}$ for the adsorption of dyes in single and binary system onto AFMCNT are plotted (Fig. 7). The k_p, I, and correlation coefficients were calculated from these plots and are given in Table 3.

The linear fit between the t/q_t vs. contact time (t) and calculated correlation coefficients (R^2) for pseudo-second-order kinetics model show that the dye

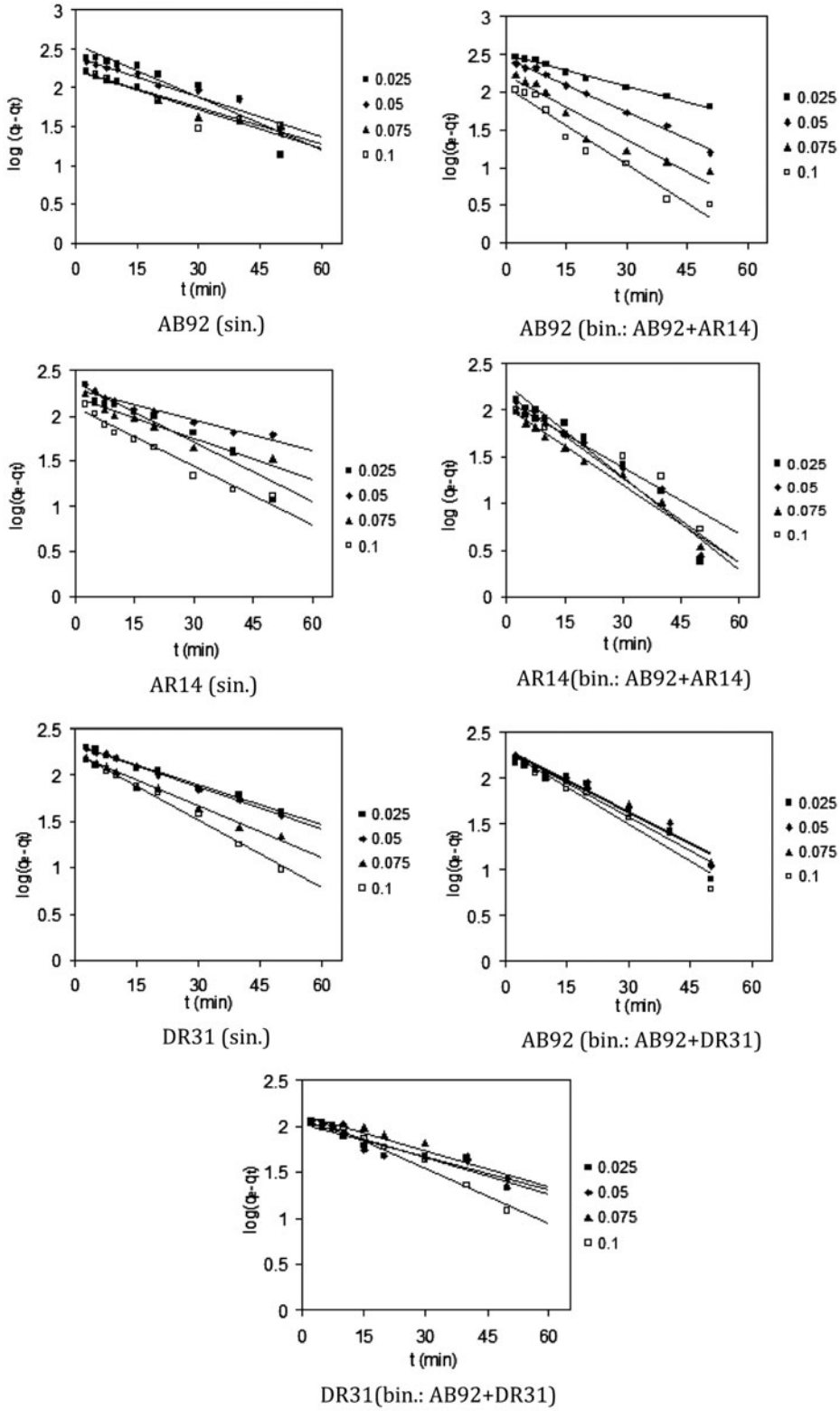

Fig. 5. The pseudo-first-order kinetics of dye removal by AFMCNT from single and binary systems.

Table 3
Linearized kinetics coefficients of dye removal using AFMCNT at different adsorbent dosages from single and binary systems

					Pseudo-first order			Pseudo-second order			Intraparticle diffusion		
	Dye		Adsorbent (g)	$(q_e)_{Exp}$	$(q_e)_{Cal}$	k_1	R^2	$(q_e)_{Cal}$	k_2	R^2	k_p	I	R^2
Single system	AB92		0.025	313	353	0.050	0.866	259	0.0003	0.947	39	9	0.988
			0.050	289	253	0.039	0.933	345	0.0002	0.949	35	13	0.981
			0.075	248	168	0.045	0.95	286	0.0003	0.984	30	22	0.995
			0.100	230	168	0.034	0.966	256	0.0003	0.981	26	29	0.975
	AR14		0.025	358	230	0.050	0.924	385	0.0004	0.988	1	123	0.953
			0.050	337	200	0.026	0.946	345	0.0004	0.974	30	90	0.956
			0.075	284	175	0.034	0.990	294	0.0005	0.991	25	90	0.955
			0.100	241	130	0.048	0.962	256	0.0008	0.998	20	100	0.913
	DR31		0.025	306	213	0.030	0.988	333	0.0003	0.974	31	54	0.987
			0.050	282	214	0.030	0.996	312	0.0002	0.972	31	34	0.991
			0.075	244	166	0.040	0.986	270	0.0004	0.990	25	53	0.975
			0.100	228	178	0.050	0.991	333	0.0004	0.986	20	50	0.986
Binary system	AB92+AR14	AB92	0.025	291	229	0.039	0.964	345	0.0002	0.986	36	20	0.947
			0.050	278	243	0.044	0.992	344	0.0002	0.976	36	6	0.970
			0.075	312	243	0.066	0.990	235	0.0002	0.971	33	1	0.940
			0.100	202	195	0.072	0.982	263	0.0002	0.971	28	9	0.990
		AR14	0.025	202	190	0.075	0.945	227	0.0006	0.989	22	49	0.888
			0.050	196	152	0.069	0.950	213	0.0005	0.983	20	38	0.975
			0.075	169	109	0.064	0.978	179	0.0007	0.988	17	41	0.952
			0.100	148	125	0.050	0.943	169	0.0006	0.986	17	25	0.988
	AB92+DR31	AB92	0.025	228	206	0.056	0.941	263	0.0003	0.969	26	8	0,987
			0.050	225	215	0.050	0.969	278	0.0002	0.983	29	11	0.989
			0.075	217	202	0.061	0.954	270	0.0002	0.989	28	8	0.979
			0.100	202	203	0.052	0.954	256	0.0002	0.995	30	7	0.967
		DR31	0.025	297	114	0.030	0.896	270	0.0009	0.987	17	131	0.936
			0.050	261	109	0.020	0.896	261	0.0009	0.987	17	124	0.932
			0.075	252	135	0.020	0.909	256	0.0006	0.967	17	100	0.920
			0.100	221	141	0.040	0.973	238	0.0007	0.984	19	74	0.980

removal kinetics can be approximated as pseudo-second-order kinetics (Table 3). In addition, the experimental q_e ($(q_e)_{Exp}$) values agree with the calculated ones ($(q_e)_{Cal}$), obtained from the linear plots of pseudo-second-order kinetics (Table 3).

3.4. Effect of operational parameters

3.4.1. Effect of adsorbent dosage

A given mass of AFMCNT can adsorb only a fixed amount of dye. Thus, the initial dosage of AFMCNT is very important. The effect of AFMCNT dosage on dye removal from single and binary systems is shown in Fig. 8. The percentage of dye removal increased with the AFMCNT dosage up to a certain limit and then it reached a constant value. The increase in adsorption of dyes with AFMCNT dosage was due to the availability of more active surface sites of AFMCNT for dye adsorption [6].

3.4.2. pH

The effect of pH on the adsorption of dyes onto AFMCNT is shown in Fig. 9. The results showed that the adsorption capacity increases when the pH is decreased. Maximum adsorption of anionic dyes occurs at acidic pH (pH 2). The electrostatic attraction as well as the organic property and structure of dye molecules and AFMCNT could play very important roles in dye adsorption on AFMCNT. At pH 2, a significantly high electrostatic attraction exists between the positively charged surfaces of the adsorbent, due to the ionization of functional groups of adsorbent and negatively charged anionic dye. As the pH of the system increases, the number of positively charged sites decreases. It does not favor the adsorption of anionic dyes due to the decrease of electrostatic attraction. The effective pH was 2 and it was used in further studies.

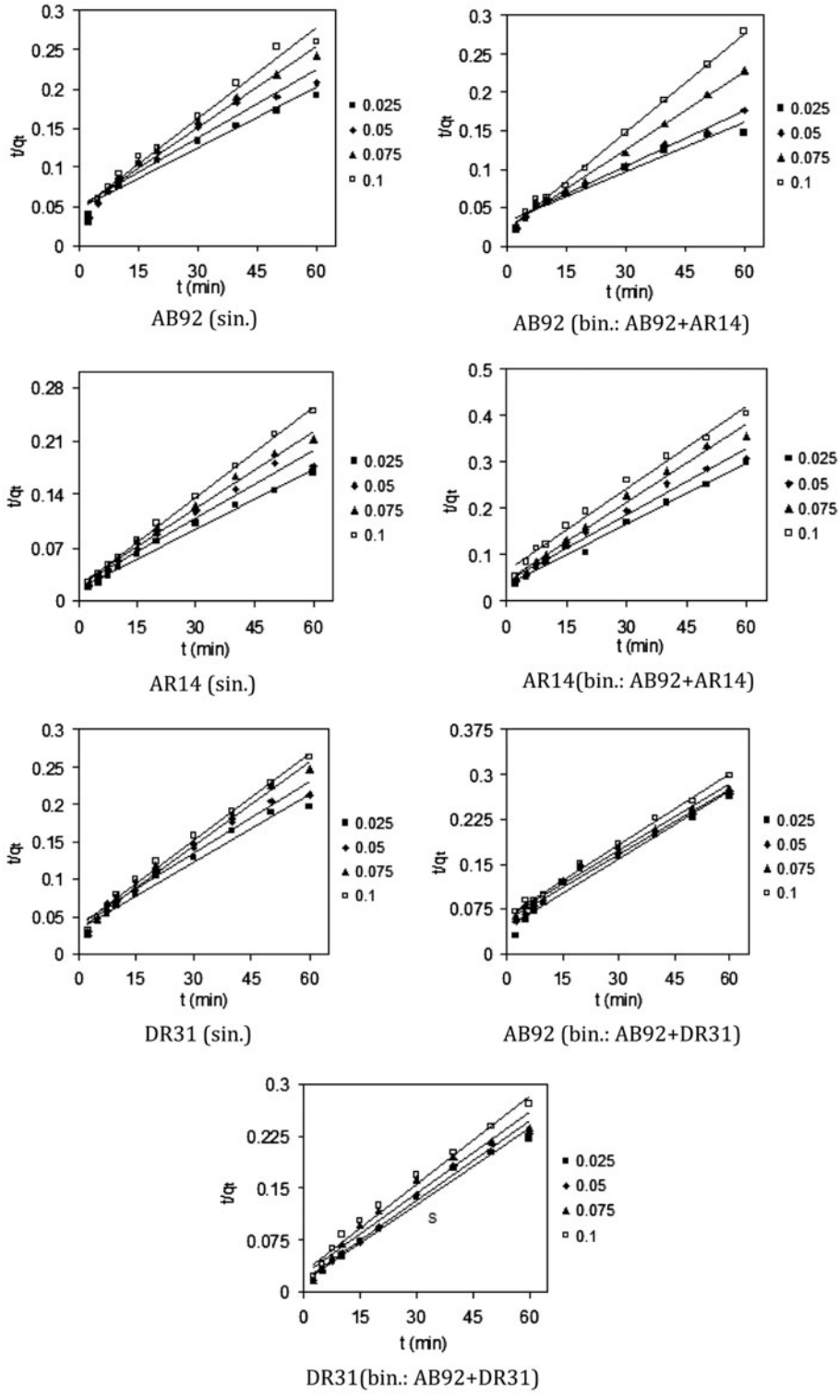

Fig. 6. The pseudo-second-order kinetics of dye removal by AFMCNT from single and binary systems.

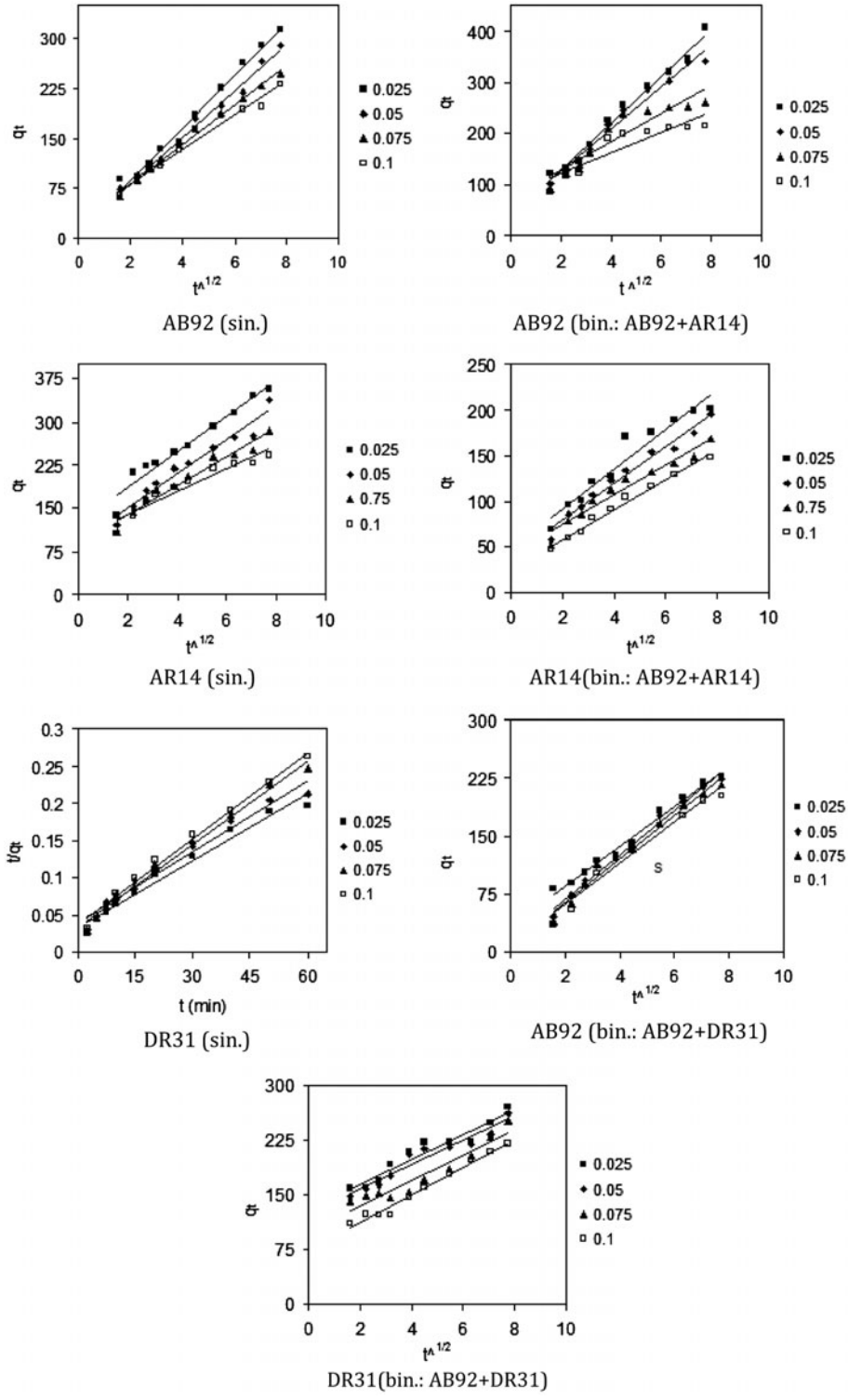

Fig. 7. The intraparticle diffusion kinetics of dye removal by AFMCNT from single and binary systems.

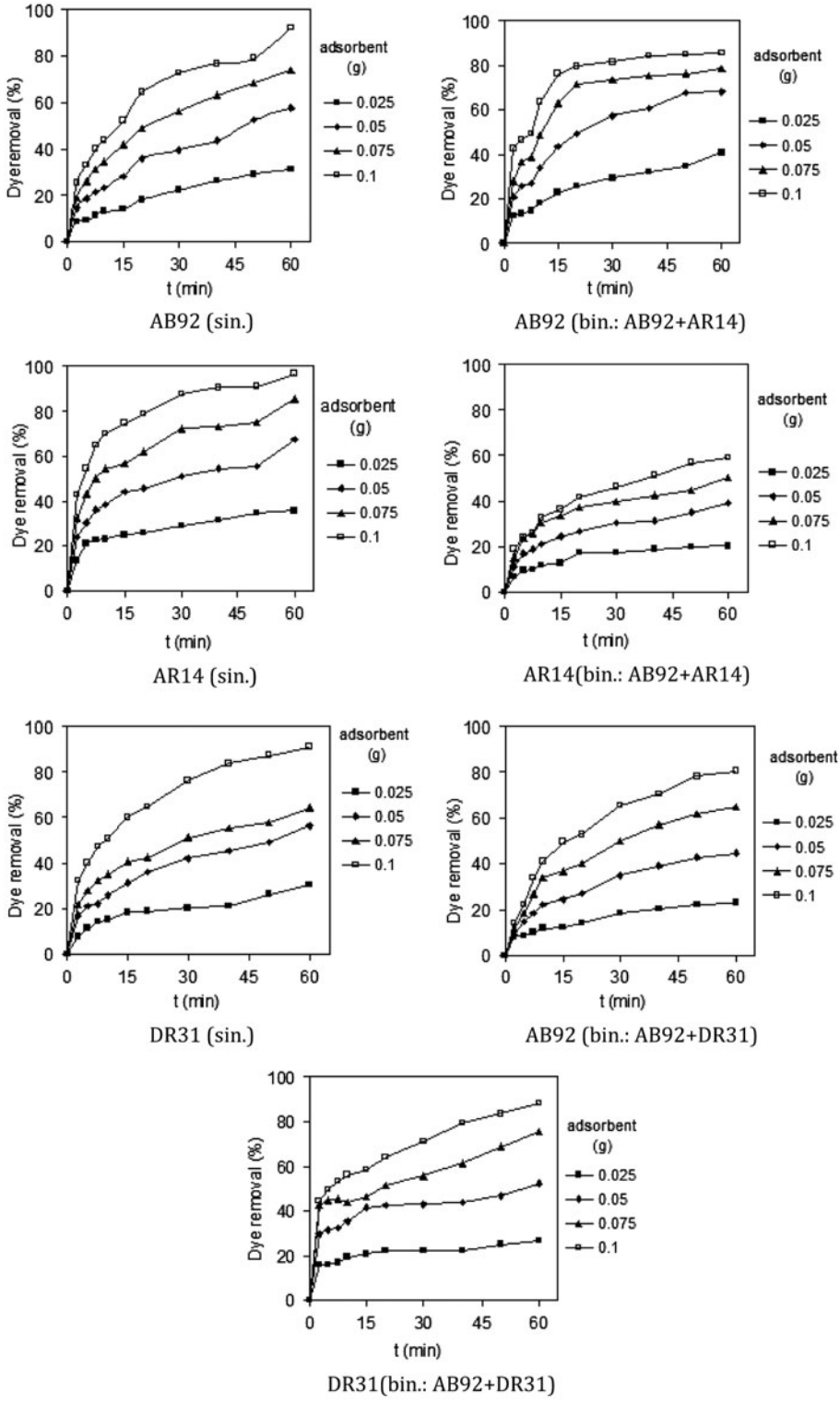

Fig. 8. The effect of adsorbent dosage (g) on dye removal by AFMCNT from single and binary systems.

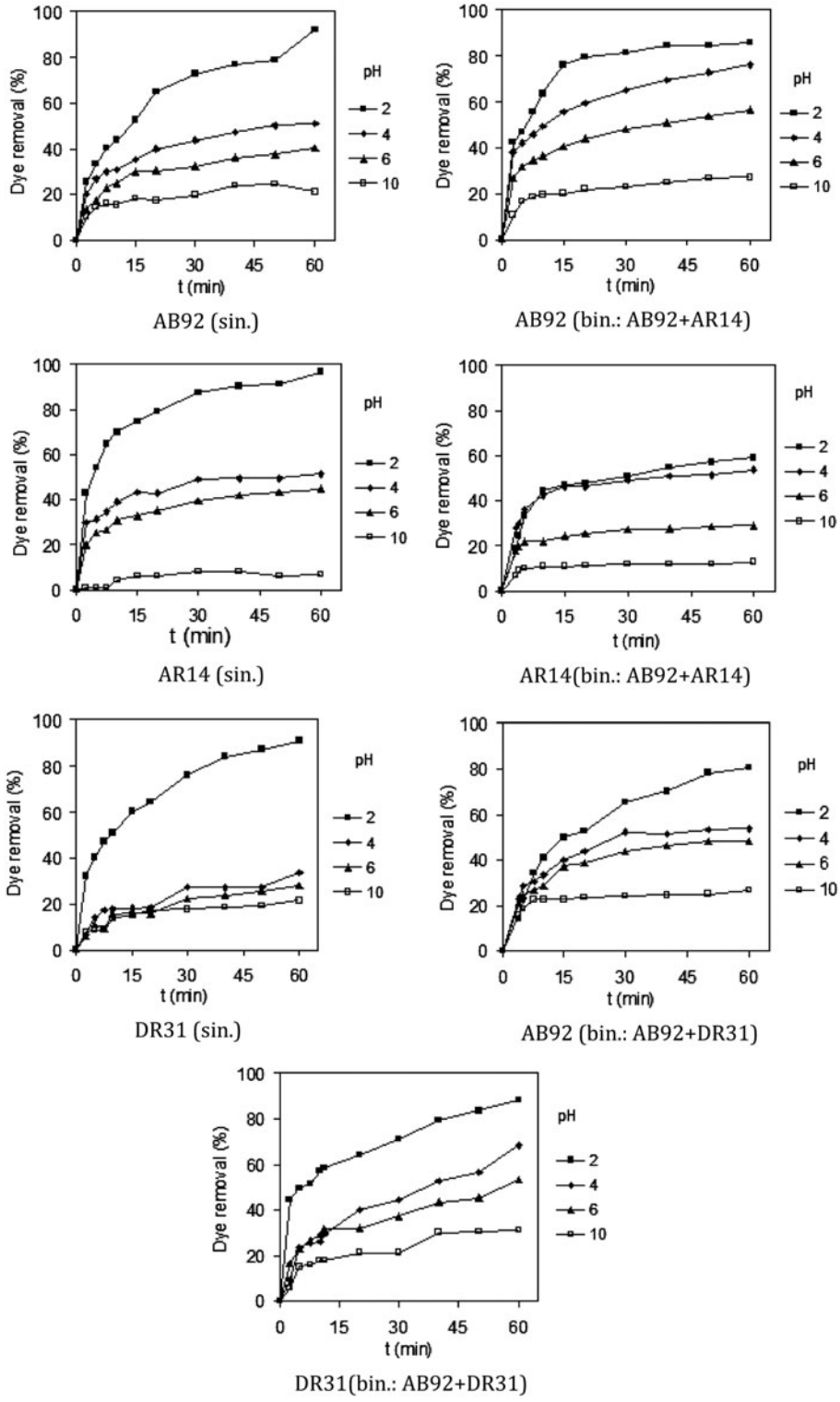

Fig. 9. The effect of pH on dye removal by AFMCNT from single and binary systems.

4. Conclusion

In this manuscript, the AFMCNT was synthesized and used to remove anionic dyes from single and binary systems. Acid Blue 92 (AB92), Acid Red 14 (AR14), and Direct Red 31 (DR31) were used as dye models. AFMCNT exhibited adsorption capacity towards anionic dyes. The equilibrium data were correlated reasonably well by Langmuir adsorption isotherm. The data indicated that the adsorption kinetics of dyes on AFMCNT followed the pseudo-second order. Dye removal increased with the AFMCNT dosage up to a certain limit and then it reached a constant value. The adsorption capacity of AFMCNT increases when the pH is decreased. The results showed that AFMCNT can be effectively used as an adsorbent for the removal of anionic dyes from binary systems.

References

[1] V.K. Gupta, R. Kumar, A. Nayak, T.A. Saleh, M.A. Barakat, Adsorptive removal of dyes from aqueous solution onto carbon nanotubes: A review, Adv. Colloid Interface Sci. 193–194 (2013) 24–34.

[2] M.Y. Nassar, I.S. Ahmed, Template-free hydrothermal derived cobalt oxide nanopowders: Synthesis, characterization, and removal of organic dyes, Mater. Res. Bull. 47 (2012) 2638–2645.

[3] Y. Bulut, N. Gözübenli, H. Aydın, Equilibrium and kinetics studies for adsorption of direct blue 71 from aqueous solution by wheat shells, J. Hazard. Mater. 144 (2007) 300–306.

[4] J.-Gang Yu, X.-H. Zhao, H. Yang, X.-H. Chen, Q. Yang, L.-Y. Yu, J.-H. Jiang, X.-Q. Chen, Aqueous adsorption and removal of organic contaminants by carbon nanotubes, Sci. Total Environ. 482–483 (2014) 241–251.

[5] A. Akyol, O.T. Can, E. Demirbas, M. Kobya, A comparative study of electrocoagulation and electro-Fenton for treatment of wastewater from liquid organic fertilizer plant, Sep. Purif. Technol. 112 (2013) 11–19.

[6] G. Crini, P.M. Badot, Application of chitosan, a natural aminopolysaccharide, for dye removal from aqueous solutions by adsorption processes using batch studies: A review of recent literature, Prog. Polym. 33 (2008) 399–447.

[7] N.M. Mahmoodi, M. Bashiri, S.J. Moeen, Synthesis of nickel–zinc ferrite magnetic nanoparticle and dye degradation using photocatalytic ozonation, Mater. Res. Bull. 47 (2012) 4403–4408.

[8] N.M. Mahmoodi, Equilibrium, kinetic and thermodynamic of dye removal using alginate from binary system, J. Chem. Eng. Data 56 (2011) 2802–2811.

[9] N.M. Mahmoodi, Photocatalytic ozonation of dyes using multiwalled carbon nanotube, Mol. Catal. A Chem. 366 (2013) 254–260.

[10] C. Lu, Y.L. Chung, Adsorption of trihalomethanes from water with carbon nanotubes, Water Res. 39 (2005) 1183–1189.

[11] H. Yan, A. Gong, H. He, J. Zhou, Y. Wei, L. Lv, Adsorption of microcystins by carbon nanotubes, Chemosphere 62 (2006) 142–148.

[12] Y.H. Li, S. Wang, A. Cao, D. Zhao, X. Zhang, C. Xu, Z. Luan, D. Ruan, J. Liang, D. Wu, B. Wei, Adsorption of fluoride from water by amorphous alumina supported on carbon nanotubes, Chem. Phys. Lett. 350 (2001) 412–416.

[13] Y.H. Li, S. Wang, J. Wei, X. Zhang, C. Xu, Z. Luan, D. Wu, B. Wei, Lead adsorption on carbon nanotubes, Chem. Phys. Lett. 357 (2002) 263–266.

[14] C. Chen, X. Wang, Adsorption of Ni(II) from aqueous solution using oxidized multiwall carbon nanotubes, Ind. Eng. Chem. Res. 45 (2006) 9144–9149.

[15] X. Peng, Z. Luan, J. Ding, Z. Di, Y. Li, B. Tia, Ceria nanoparticles supported on carbon nanotubes for the removal of arsenate from water, Mater. Lett. 59 (2005) 399–403.

[16] S. Iijima, Helical microtubules of graphitic carbon, Nature 354 (1991) 56–58.

[17] N. Jha, S. Ramaprabhu, Thermal conductivity studies of metal dispersed multiwalled carbon nanotubes in water and ethylene glycol based nanofluids, J. Appl. Phys. 106 (2009) 84317–84326.

[18] R.D. Ambashta, M. Sillanpää, Water purification using magnetic assistance: A review, J. Hazard. Mater. 180 (2010) 38–49.

[19] A.F. Ngomsik, A. Bee, M. Draye, G. Cote, V. Cabuil, Magnetic nano- and microparticles for metal removal and environmental applications: A review, C.R. Chimie. 8 (2005) 963–970.

[20] J. Sun, R. Xu, Y. Zhang, M. Ma, N. Gu, Magnetic nanoparticles separation based on nanostructures, J. Magn. Magn. Mater. 312 (2007) 354–358.

[21] K.K.H. Choy, J.F. Porter, G. McKay, Langmuir isotherm models applied to the multicomponent sorption of acid dyes from effluent onto activated carbon, J. Chem. Eng. Data 45 (2000) 575–584.

[22] D.L. Pavia, G.M. Lampman, G.S. Kaiz, Introduction to Spectroscopy: A Guide for Students of Organic Chemistry, W.B Saunders Company, New York, NY, 1987.

[23] S. Maensiri, C. Masingboon, B. Boonchom, S. Seraphin, A simple route to synthesize nickel ferrite ($NiFe_2O_4$) nanoparticles using egg white, Scr. Mater. 56 (2007) 797–800.

[24] M. Mouallem-Bahout, S. Bertrand, O. Pena, Synthesis and characterization of $Zn_{1-x}Ni_xFe_2O_4$ spinels prepared by a citrate precursor, J. Solid State Chem. 178 (2005) 1080–1086.

[25] V.A.M. Brabers, Infrared spectra of cubic and tetragonal manganese ferrites, Phys. Stat. Sol. 33 (1969) 563–572.

[26] S. Hafner, Z. Krist, Order/disorder and I.R.-absorption. IV. The absorption of some metal oxides with spinel structure (Ordnung/unordnung und ultrarotabsorption IV, die absorption einiger metalloxyde mit spinellstruktur), Scr. Mater. 115 (1961) 331–358.

[27] R.D. Waldron, Infrared spectra of ferrites, Phys. Rev. 99 (1955) 727–735.

[28] P. Duran, J. Tartaj, F. Rubio, C. Moure, O. Pena, Synthesis and sintering behavior of spinel-type $Co_xNiMn_{2-x}O_4 (0.2 \le \times \le 1.2)$ prepared by the ethylene glycol–metal nitrate polymerized complex process, Ceram. Int. 31 (2005) 599–610.

[29] J.L. Gong, B. Wang, G.M. Zeng, C.P. Yang, C.G. Niu, Q.Y. Niu, W.J. Zhou, Y. Liang, Removal of cationic dyes from aqueous solution using magnetic multi-wall carbon nanotube nanocomposite as adsorbent, J. Hazard. Mater. 164 (2009) 1517–1522.
[30] I. Langmuir, The constitution and fundamental properties of solids and liquids. Part I: Solids, J. Am. Chem. Soc. 38 (1916) 2221–2295.
[31] H.M.F. Freundlich, Uber die adsorption in lasugen, Z. Phys. Chem. (Leipzig) 57 (1906) 385–470.
[32] E.R. Alley, Water Quality Control Handbook, McGraw-Hill Education, London, 2000.
[33] M.J. Temkin, V. Pyzhev, Recent modification to Langmuir isotherms, Acta Physiochim. 12 (1940) 217–222.
[34] Y.C. Kim, I. Kim, S. Rengraj, J. Yi, Arsenic removal using mesoporous alumina prepared via a templating method, Environ. Sci. Technol. 38 (2004) 924–931.
[35] S. Wang, C. Wei Ng, W. Wang, Q. Li, Z. Hao, Synergistic and competitive adsorption of organic dyes on multiwalled carbon nanotubes, Chem. Eng. J. 197 (2012) 34–40.
[36] M. Shirmardi, A. Mesdaghinia, A.H. Mahvi, S. Nasseri, R. Nabizadeh, Kinetics and equilibrium studies on adsorption of acid red 18 (azo-dye) using multiwall carbon nanotubes(MWCNTs) from aqueous solution, E.-J. Chem. 9 (2012) 2371–2383.
[37] S.B. Wang, C.W. Ng, W.T. Wang, Q. Li, L.Q. Li, A comparative study on the adsorption of acid and reactive dyes on multiwall carbon nanotubes in single and binary dye systems, J. Chem. Eng. Data 57 (2012) 1563–1569.
[38] W. Konicki, I. Pelech, E. Mijowska, I. Jasinska, Adsorption of anionic dye direct red 23 onto magnetic multi-walled carbon nanotubes–Fe_3C nanocomposite: Kinetics, equilibrium and thermodynamics, Chem. Eng. J. 210 (2012) 87–95.
[39] N.M. Mahmoodi, Magnetic ferrite nanoparticle—alginate composite: Synthesis, characterization and binary system dye removal, J. Taiwan Inst. Chem. Eng. 44 (2013) 321–329.
[40] S. Lagergren, Arsenic removal using mesoporous alumina prepared via a templating method, K. Sven. Vetenskapsakad. Handl. 24 (1898) 1–39.
[41] Y.S. Ho, Adsorption of Heavy Metals from Waste Streams by Peat, PhD Thesis, The University of Birmingham, Birmingham, 1995.
[42] W.J. Weber, J.C. Morris, Kinetics of adsorption on carbon from solution, J. Sanitary Eng. Div. Am. Soc. Civ. Eng. 89 (1963) 31–60.
[43] Ç.O. Ay, A.S. Özcan, Y. Erdoğan, A. Özcan. Characterization of *Punica granatum* L. peels and quantitatively determination of its biosorption behavior towards lead(II) ions and Acid Blue 40, Colloids Surf. B. 100 (2012) 197–204.